

A MAP OF OMC-1 IN CO $J=9 \rightarrow 8$

DANIEL P. MARRONE¹, JAMES BATTAT¹, FRANK BENSCH^{1,2}, RAYMOND BLUNDELL¹, MARCOS DIAZ³, HUGH GIBSON^{1,4},
TODD HUNTER¹, DENIS MELEDIN^{1,5}, SCOTT PAINE¹, D. COSMO PAPA¹, SIMON RADFORD⁶, MICHAEL SMITH¹, AND
EDWARD TONG¹

Draft version November 3, 2018

ABSTRACT

The distribution of $^{12}\text{C}^{16}\text{O } J=9 \rightarrow 8$ (1.037 THz) emission has been mapped in OMC-1 at 35 points with $84''$ resolution. This is the first map of this source in this transition and only the second velocity-resolved ground-based observation of a line in the THz frequency band. There is emission present at all points in the map, a region roughly $4' \times 6'$ in size, with peak antenna temperature dropping only near the edges. Away from the Orion KL outflow, the velocity structure suggests that most of the emission comes from the OMC-1 photon-dominated region, with a typical line width of 3-6 km s^{-1} . Large velocity gradient modeling of the emission in $J=9 \rightarrow 8$ and six lower transitions suggests that the lines originate in regions with temperatures around 120 K and densities of at least $10^{3.5} \text{ cm}^{-3}$ near $\theta^1\text{C Ori}$ and at the Orion bar, and from 70 K gas at around 10^4 cm^{-3} southeast and west of the bar. These observations are among the first made with the 0.8 m Smithsonian Astrophysical Observatory Receiver Lab Telescope, a new instrument designed to observe at frequencies above 1 THz from an extremely high and dry site in northern Chile.

Subject headings: ISM: clouds – ISM: individual: OMC-1 – ISM: individual: Orion Kleinmann-Low – ISM: individual: Orion Bar – submillimeter – telescopes

1. INTRODUCTION

The OMC-1 region of the Orion A molecular cloud is the nearest site (~ 500 pc) of recent high mass star formation. Its diverse components make it a natural laboratory for the study of many stages of star formation. The OMC-1 cloud is one of three clouds connected by the Orion “ridge,” a long and dense molecular filament (Castets et al. 1990). The H II regions M42 and M43 sit in front of the ridge, and extended narrow-line CO emission (the “spike” component) is excited in the photon-dominated region (PDR) at the interface between the ionized and neutral gas. The brightest star in the Trapezium, $\theta^1\text{C Ori}$, is the dominant source for the far-ultraviolet photons that sustain the M42 H II region and its associated PDR (Stacey et al. 1993). One arcminute to the north-west of $\theta^1\text{C Ori}$, the Kleinmann-Low nebula (KL) is the brightest source outside the solar system at $20 \mu\text{m}$, with a luminosity of $\sim 10^5 L_{\odot}$ (Kleinmann & Low 1967). Several powerful sources have been identified in the infrared within KL, including the Becklin-

Neugebauer point source (BN; Becklin & Neugebauer 1967), likely a runaway B star (Plambeck et al. 1995; Tan 2004), and IRC2, once thought to be the power source for the nebula (Downes et al. 1981) but more recently resolved into several sources that may not be self-luminous (Dougados et al. 1993; Menten & Reid 1995; Gezari et al. 1998). Molecular line observations of Orion KL show emission extending out to nearly $\pm 100 \text{ km s}^{-1}$ (e.g., CO $J=7 \rightarrow 6$ and $J=4 \rightarrow 3$ in Wilson et al. 2001, hereafter WMKH01). This large line width, usually called “plateau” emission, is due to an outflow long attributed to IRC2 (Wright et al. 1983) that is more likely associated with nearby radio and infrared point sources (Menten & Reid 1995; Greenhill et al. 1998). The Orion bar is a well studied region of the PDR south-east of the Trapezium. At this location the ionization front is viewed edge-on over a length of $\sim 3'$, allowing direct examination of the chemical stratification in a plane-parallel PDR (e.g., van der Werf et al. 1996; Walmsley et al. 2000).

The OMC-1 cloud has been mapped in many millimeter, submillimeter, and far-IR transitions (e.g., Stacey et al. 1993; Goldsmith et al. 1997; Herrmann et al. 1997; Plume et al. 2000; Sempere et al. 2000; Ikeda et al. 2002; WMKH01). Previous observations in CO transitions up to $J=7 \rightarrow 6$ (Schulz et al. 1995; WMKH01) have found warm PDR gas extending over a very large region. In this paper we present the first map of OMC-1 in the $J=9 \rightarrow 8$ transition of $^{12}\text{C}^{16}\text{O}$. This line has previously been observed in OMC-1 from the Kuiper Airborne Observatory (Röser 1991; Betz & Boreiko 1993) and from the Heinrich Hertz Submillimeter Telescope (Kawamura et al. 2002), but never at more than a few points. Our map contains 35 pointings and covers $\sim 25 \text{ arcmin}^2$ at $84''$ resolution. Our spectra provide information about the population of the $J=9$ rotational level (250 K), nearly 100 K higher than the $J=7$ level probed by $J=7 \rightarrow 6$ maps, and the

¹ Harvard-Smithsonian Center for Astrophysics, 60 Garden Street, Cambridge, MA 02138; dmarrone@cfa.harvard.edu (corresponding author), j battat@cfa.harvard.edu, rblundell@cfa.harvard.edu, thunter@cfa.harvard.edu, spaine@cfa.harvard.edu, cpapa@cfa.harvard.edu, msmith@cfa.harvard.edu, etong@cfa.harvard.edu.

² Current address: Radioastronomisches Institut der Universität Bonn, Auf dem Hügel 71, D-53121 Bonn, Germany; fbensch@astro.uni-bonn.de.

³ Boston University, Department of Electrical and Computer Engineering, 8 St. Mary’s Street, Boston, MA 02215; mardiaz@bu.edu.

⁴ Current address: RPG Radiometer Physics GmbH, Birkenmaarstrasse 10, 53340 Meckenheim, Germany; hgibson@cfa.harvard.edu.

⁵ Current address: GARD/MC2, Fysikgrand 3, Chalmers University of Technology, S-412 96 Gothenburg, Sweden; meledin@oso.chalmers.se.

⁶ National Radio Astronomy Observatory, 949 North Cherry Avenue, Tucson, AZ 85721; sradford@nrao.edu

critical density at $J = 9 \rightarrow 8$ ($\sim 10^6 \text{ cm}^{-3}$) is approximately twice that at $J = 7 \rightarrow 6$ ($\sim 5 \times 10^5 \text{ cm}^{-3}$). This THz transition should therefore be a better probe of the density and temperature of warm and dense sources such as OMC-1, where lower transitions are thermalized.

Because of absorption by the Earth’s atmosphere, the $J = 9 \rightarrow 8$ transition of CO as well as other astronomically interesting lines at frequencies above 1 THz are unobservable from current ground-based observatories except in very unusual weather. However, recent atmospheric measurements have demonstrated that several windows can open up between 1 and 3 THz at very high and dry locations (Paine et al. 2000; Matsushita et al. 1999). Under favorable conditions, three of these windows, centered at 1.03, 1.35, and 1.5 THz, show transmission as high as 40%. These windows include six rotational transitions of ^{12}CO and ^{13}CO , as well as the ground-state fine-structure transition of singly ionized nitrogen, one of the most important coolants of the diffuse ISM, and numerous other common and exotic atomic and molecular lines. A new telescope, the Receiver Lab Telescope (RLT), has been constructed by the Smithsonian Astrophysical Observatory to take advantage of these windows, and is currently deployed at 5525 m altitude in northern Chile. This map of OMC-1 represents some of the first observations made with the RLT and demonstrates the capabilities of this new instrument.

2. OBSERVATIONS

We observed the OMC-1 region of the Orion A molecular cloud in the $J = 9 \rightarrow 8$ transition of $^{12}\text{C}^{16}\text{O}$ using the 0.8 m diameter RLT (Blundell et al. 2002) on Cerro Sairecabur, Chile. At the 1036.912 GHz frequency of this line we expect a beamsize of $84''$. Our 330 channel autocorrelation spectrometer has a bandwidth of 286 km s^{-1} (990 MHz) and a resolution of 1.04 km s^{-1} at this frequency. The data were acquired on the morning of 2002 December 15 between 05:30 and 07:30 UT. We obtained spectra at 35 points with $50''$ spacing in an irregularly shaped region of OMC-1. These observations were made in position-switching mode with a reference point $10''$ to the west of each map point. Each spectrum is the sum of 12 integration cycles of 5 s on-source and 5 s off-source. The map is centered on $\alpha = 05^{\text{h}}35^{\text{m}}14^{\text{s}}$ and $\delta = -05^{\circ}22'31''$ (J2000.0), which coincides with the location of several Orion line surveys (Sutton et al. 1985; Blake et al. 1986; Schilke et al. 2001). Orion KL, BN, and IRc2 are all well within the beam at this location. The ranges in offsets from the map center are $\Delta\alpha = -50''$ to $+150''$ and $\Delta\delta = -250''$ to $+100''$.

The telescope pointing varies from night to night by up to tens of arcseconds because of shifts in the telescope foundation. To remove these variations we used an optical guidescope to determine offsets from our base pointing model. The limitation of this method is the accuracy with which we know the offset between the optical and radio beams, about $15''$, and we take this value to be our absolute pointing error. Within the map the relative pointing is considerably better. To ensure that there was no systematic drift in the $(0'', 0'')$ point over the observation period we remeasured the pointing offsets on a nearby star approximately every 25 minutes. We also measured the center spectrum twice; the two measurements were separated by 1 hr, and there were

three measurements of the pointing offsets made during that interval. As a check of the consistency of these two spectra, we rescale them so that the averages of their three highest channels are the same and compute the rms difference between them in the nonbaseline channels. When the spectra are scaled to 100 K we measure an rms difference of 4.8 K, very similar to the 4.2 K we expect from the noise seen in the baseline channels, and the difference spectrum shows no remnant structure. Adjacent spectra are significantly different; the most similar spectrum, at $(0'', -50'')$, differs from the two center-point spectra by 7.7 and 7.4 K and has narrower wings. We also note that the averages of the three highest channels are 65.5 and 64.1 K for the first and second center-point spectra, respectively, indicating that the calibration was self-consistent to 2% over this interval.

The hot electron bolometer receiver used for these measurements is described elsewhere (Meledin et al. 2004). During these observations the double-sideband receiver temperature was found to be 980 K through observations of cold (liquid nitrogen) and ambient loads. Atmospheric transmission measurements were made every 10 minutes by a Fourier transform spectrometer (Paine et al. 2000) located a few meters away from the telescope. Over the course of the observations the zenith transmission at the line frequency decreased from 23.5% to 18%. To determine a single-sideband system temperature (T_{sys}), we assume equal gain in the signal and image sidebands (centered on 1036.912 and 1030.848 GHz, respectively) because the mixer frequency response is essentially flat between 900 GHz and 1.05 THz. Our data are calibrated to the T_A^* scale of Ulich & Haas (1976). We have measured a beam efficiency (η_l in Ulich & Haas 1976) of 45% at 883 GHz by mapping a telluric ozone absorption feature against Jupiter (angular diameter $42''$; Marrone et al. 2004). This efficiency is much lower than expected; the RLT primary mirror has an rms figure error of only $3 \mu\text{m}$, causing a 2% Ruze loss, and our blockage and illumination pattern give a theoretical efficiency of 94%. We believe that this indicates that the receiver was poorly aligned with the telescope and that a significant portion of the receiver beam was being truncated before reaching the secondary mirror. We have not made this beam measurement nearer to the CO $J = 9 \rightarrow 8$ frequency, so we adopt this efficiency for the calibration. After accounting for the above factors, the single-sideband system temperature at the source elevation increased from 2.7×10^4 to 6.4×10^4 K during our observations as the transmission degraded and Orion set. From estimates of the uncertainties in the atmospheric transmission and the efficiency, we expect that our calibration is accurate to $\pm 25\%$.

3. RESULTS

The calibrated spectrum at each of the 35 map points is shown in Figure 1 superposed on a contour map of the CO $J = 9 \rightarrow 8$ line flux integrated between -30 and $+40 \text{ km s}^{-1}$. The narrow spike emission from the PDR is evident throughout the map, while broad plateau emission is only observed near the center, around Orion KL. Linear baselines were fitted to 27 channels (-47 to -30 km s^{-1} and $+40$ to $+47 \text{ km s}^{-1}$) in each spectrum and removed. Because of mismatched baselines in the output of the three independent sections of our auto-

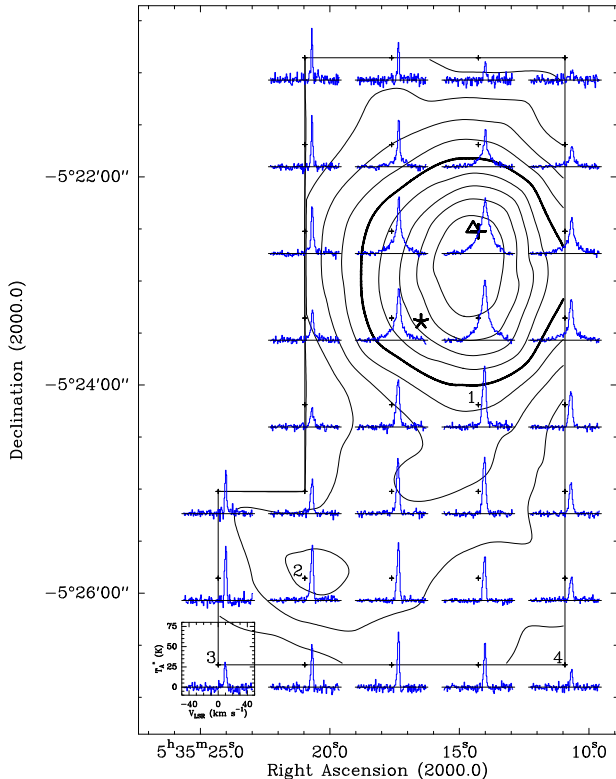


FIG. 1.— CO $J = 9 \rightarrow 8$ emission in OMC-1. The contours trace the line flux between -30 and $+40$ km s^{-1} (in K km s^{-1}). The contours are spaced by 10% of the peak flux (1260 K km s^{-1} near the center point) and run from 10 to 90%, with the 50% contour reinforced. The small crosses mark the location of map pointings, and the bold cross marks the center point of the map at $\alpha = 05^{\text{h}}35^{\text{m}}14^{\text{s}}$, $\delta = -05^{\circ}22'31''$ (J2000.0). The individual spectra lie on a square grid with $50''$ spacing. The star marks the position of $\theta^1\text{C Ori}$, and the triangle marks the position of the IRC2 complex of sources. The numbers 1-4 correspond to the positions in Tables 1 and 2. The spectrum at each map point is also plotted. The scale for each spectrum is the same as that given in the lower left.

correlation spectrometer, it was only possible to use the middle 110 channels (covering -47 to $+47$ km s^{-1}) in our final spectra. Unfortunately, other observations of Orion KL in this transition (Röser 1991; Betz & Boreiko 1993; Kawamura et al. 2002) and lower transitions (e.g., Schulz et al. 1995; WMKH01) show plateau emission at velocities outside the -30 to $+40$ km s^{-1} range. Hence, the baselines subtracted from the ($\Delta\alpha = 0''$, $= 0''$) and ($0''$, $-50''$) spectra, where the emission is widest in velocity, are likely to be inaccurate, and the integrated emission obtained from these spectra is significantly diminished.

Figure 1 shows that the peak emission in the $J = 9 \rightarrow 8$ line is $\sim 20''$ south of our map center. Observations of lower CO transitions, from $J = 1 \rightarrow 0$ and $J = 2 \rightarrow 1$ (Castets et al. 1990) to $J = 7 \rightarrow 6$ (Howe et al. 1993; WMKH01), show peak emission at the location of IRC2, marked with the triangle in Figure 1. The addition of reasonable flux corrections at the two central points affected by the baseline problem can move the center point toward ($0''$, $0''$) by as much as $10''$. The remaining error is consistent with our absolute pointing uncertainty of $15''$.

The outflow near IRC2 is unresolved in our map, as expected from its $\sim 50''$ size in $J = 7 \rightarrow 6$ (WMKH01). We have used the emission in the line wings, which is spatially confined to this outflow, as a source to map the beam and estimate the beam size. For this estimate we assume Gaussian profiles for the source and beam, the simplest possible assumption. We obtain a range of half-power widths between $85''$ and $105''$, which, after deconvolution with a $50''$ source, give beam sizes between $69''$ and $92''$. These values provide confirmation that the telescope beam is similar to the $84''$ we predict from the telescope and receiver optics design.

4. DISCUSSION

4.1. Radiative Transfer Modeling

CO $J = 9 \rightarrow 8$ emission is present over the entire mapped region, and the peak line temperature decreases only at the edges. WMKH01 also found $J = 7 \rightarrow 6$ emission over their entire (slightly smaller) mapping region. As mentioned previously, we expect the $J = 9 \rightarrow 8$ line to be a better probe of the warm and dense OMC-1 PDR. To examine the conditions in the PDR, we compare the emission in this line to that in lower transitions: $^{12}\text{CO } J = 7 \rightarrow 6$ and $J = 4 \rightarrow 3$ (WMKH01), $J = 6 \rightarrow 5$ (K. N. Allers 2005, in preparation), $J = 3 \rightarrow 2$ (Tigges 1993), $^{13}\text{CO } J = 3 \rightarrow 2$ (Tigges 1993), and $J = 1 \rightarrow 0$ (Plume et al. 2000). The data sets have been convolved to the $84''$ resolution of the RLT, except for the $J = 6 \rightarrow 5$ data, which have $86''$ resolution. We estimate the density and temperature at various map points using the large velocity gradient (LVG) model of Stutzki & Winnewisser (1985). LVG models assume that ordered line-of-sight motions are large compared to local random velocities and that there is a one-to-one correspondence between position along the line of sight and velocity, allowing the radiative transfer to be treated locally (Scoville & Solomon 1974). The free parameters in these models are: the molecular hydrogen density [$n(\text{H}_2)$, or simply n], the CO column density per velocity interval (dN/dv), and the kinetic temperature (T_{kin}). The model performs calculations through $J = 20$ with the H_2 -CO collision coefficients of Flower & Launay (1985). Four representative points were selected from the map (marked in Figure 1); the Rayleigh-Jeans main-beam brightness temperatures in each transition at each position are given in Table 1. To correct the $J = 9 \rightarrow 8$ data from T_A^* to T_{MB} , we use a source coupling efficiency of 85% because of the extended nature of the spike emission. This is the same coupling efficiency used with the $J = 6 \rightarrow 5$ data by K. N. Allers (2005, in preparation) for a similar beam size. Coupling efficiencies for the other data are obtained from the original papers. Position 1 is near $\theta^1\text{C Ori}$, position 2 lies on the Bar, and positions 3 and 4 fall on the edges of the mapped region where the $J = 9 \rightarrow 8$ emission is decreasing.

We estimate the model parameters using a χ^2 minimization analysis. The peak brightness temperature in each line is determined from a Gaussian fit. These temperatures are compared to a grid of LVG models covering T_{kin} from 40 to 200 K, n from $10^{2.5}$ to $10^{6.5} \text{ cm}^{-3}$, and dN/dv from $10^{15.5}$ to $10^{20} \text{ cm}^{-2} \text{ s km}^{-1}$. We assign an error of 25% to each temperature to account for the uncertainty in the inter-telescope calibration and the error-beam contribution to the observed temper-

atures on this extended source. For calculations of ^{13}CO line temperatures we use a column density ratio of $N(^{12}\text{CO})/N(^{13}\text{CO}) = 67$, as determined in Orion A by Langer & Penzias (1990), and assume that the ^{12}CO and ^{13}CO emission arise in gas of the same temperature. The T_{kin} values we derive are very similar to those measured for ^{13}CO by Plume et al. (2000), where the gas kinetic temperature was determined from measurements of ^{13}CO lines only, suggesting that this assumption is a good approximation for this source.

The parameters derived from these fits are given in Table 2. The goodness of fit at each position is judged by examining the minimum value of the reduced χ^2 (χ_r^2), or χ^2 divided by the number of degrees of freedom. The ranges in the table describe the region in parameter space where χ_r^2 is less than 1 plus the minimum value. The observed minima in χ_r^2 indicate good fits at all four positions.

The fits at positions 1 and 2 provide examples of the difficulties of determining n from sets of thermalized transitions. When the ^{12}CO line temperatures at these positions are converted from the Rayleigh-Jeans scale to the Planck scale (under the assumption that they are optically thick), they are roughly constant, indicating LTE emission. In this equilibrium case, the line temperatures are no longer sensitive to density and the models can only set a lower limit to the density of the gas, that being the density required to roughly thermalize all of the observed transitions. It is only because the temperatures of the two ^{13}CO transitions are simultaneously matched only in a small region of densities that these positions have density upper bounds. Higher densities at the same column density per velocity interval are not strongly excluded because they give only slightly larger values of χ_r^2 . Positions 3 and 4 indicate the value of high- J data in dense environments. At these positions the $J = 9 \rightarrow 8$ emission is not thermalized, allowing strong constraints on the density. When we apply our fitting technique to these positions without the $J = 9 \rightarrow 8$ information we do not obtain density upper bounds.

These results match well with previous measurements, although we are able to place tighter constraints on the gas conditions. Based on ^{12}CO $J = 7 \rightarrow 6$ and ^{13}CO $J = 2 \rightarrow 1$, Howe et al. (1993) found that the CO emission could be produced by column densities per velocity interval in the range $10^{17.3} - 10^{18.6} \text{ cm}^{-2} \text{ s km}^{-1}$, densities of $10^3 - 10^5 \text{ cm}^{-3}$, and temperatures of 40–200 K. Plume et al. (2000) also used LVG models and an assumed density of 10^4 cm^{-3} to find a nearly constant ^{13}CO column density per velocity interval of $10^{16.4 \pm 0.3} \text{ cm}^{-2} \text{ s km}^{-1}$, or $10^{18.1 \pm 0.3} \text{ cm}^{-2} \text{ s km}^{-1}$ for ^{12}CO with their assumed abundance ratio, and temperatures of ~ 100 K. At all four positions we find a CO column within the range $10^{17.5} - 10^{18.3} \text{ cm}^{-2} \text{ s km}^{-1}$ and molecular hydrogen density $10^{3.5} - 10^{4.6} \text{ cm}^{-3}$, although higher densities are allowed at lower likelihood at positions 1 and 2. There are significant temperature variations over the OMC-1 cloud, with the lowest temperatures occurring at the two positions farthest from the strong UV source $\theta^1\text{C Ori}$.

4.2. Line Features

Away from the broad emission component around Orion KL, the quiescent (spike) emission dominates. Fig-

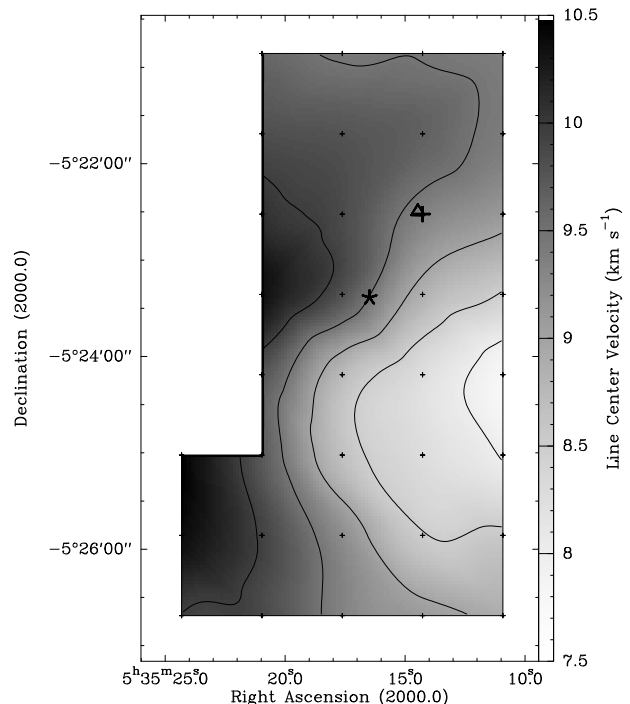


FIG. 2.— Velocity of CO $J = 9 \rightarrow 8$ emission in OMC-1. The line-center velocities are obtained from each spectrum using a Gaussian fit. A single component is used away from the KL outflow, while at the nine center positions a broad component is added but constrained to have the same velocity. Contours trace velocities from 8 to 10 km s^{-1} in steps of 0.5 km s^{-1} . Symbols are the same as in Figure 1.

ure 2 is a map of the line-center velocities obtained from Gaussian fits to the $J = 9 \rightarrow 8$ spectra. At the nine positions closest to the map center where the KL outflow is visible, we add a broad component to the fit but constrain its velocity to match that of the narrow component. As seen in lower transitions, such as the $J = 7 \rightarrow 6$, $J = 4 \rightarrow 3$, and $J = 2 \rightarrow 1$ transitions in WMKH01, there is a gradient in the line-center velocity of the spike emission. The minimum (least redshifted) velocity is approximately 7.5 km s^{-1} near $(-50'', -100'')$, increasing toward the north and southeast to more than 10 km s^{-1} at the eastern edge of the map. The observed velocities are systematically redshifted (typically $0.5\text{--}1 \text{ km s}^{-1}$) from velocities measured in the dense ridge gas (e.g., CN emission in Rodríguez-Franco et al. 2001). We interpret this as evidence that most of the CO $J = 9 \rightarrow 8$ emission arises in the PDR rather than gas deeper in the molecular cloud. The redshift between the PDR surface and the ridge may be due to the slow expansion of the H II region into the molecular cloud. Emission from the ridge, if it is present, could be visible as a blue shoulder in individual spectra, but the only spectrum that may show this second component is $(0'', -200'')$.

The FWHM of the spike emission, as measured from the Gaussian fits, narrows away from the map center, decreasing from 6 km s^{-1} (FWHM) near the KL outflow to about 3 km s^{-1} in the southeast corner and 2.5 km s^{-1} in the northeast. WMKH01 shows the line width increasing to the west at the declination of $\theta^1\text{C Ori}$ in $J = 7 \rightarrow 6$, but our angular resolution does not allow us to disentangle the KL outflow and compare directly.

Only one spectrum shows a clear emission component other than the spike and plateau at our resolution and signal-to-noise ratio. At the Orion bar [(100", -200"); position 2 above], a blue component stands out above 3 km s^{-1} . The same component may also be present at (100", -150") and (50", -200"). The emission at this location appears to be the sum of two components: one around 10.5 km s^{-1} (consistent with the velocity at the Bar), and another around 7.5 km s^{-1} ; both components are visible in the other ^{12}CO and ^{13}CO transitions as well. The ^{12}CO and ^{13}CO $J = 1 \rightarrow 0$ channel maps of Tauber et al. (1994) resolve the two components in space and velocity, with the 7.5 km s^{-1} component centered approximately 30" north and west of the bar emission. When convolved to the same angular resolution (84"), the line shape is very similar in the $J = 4 \rightarrow 3$ through $J = 9 \rightarrow 8$ transitions, suggesting that the line-center and wing components are at similar average density and temperature and differ only in beam filling factor. We suggest that the blue component may represent molecular gas left over from the disrupted near edge of the molecular cloud.

5. CONCLUSIONS

We have mapped CO $J = 9 \rightarrow 8$ emission in the OMC-1 region of the Orion A molecular cloud over a 25 arcmin^2 region at 84" resolution. The line is detected over the entire map, similar to what has been seen in other submillimeter CO transitions. The high critical density of this transition and the high energy of the $J = 9$ level make it more difficult to excite than lower levels, allowing us

to measure the molecular hydrogen density, temperature, and CO column density per velocity interval of the gas at four locations in the PDR by combining these spectra with lower transitions. We find that near the center of the map even this transition may not be high enough to strongly constrain the density because of the high gas temperatures. A wider survey of the cloud in this line or the higher rotational lines of ^{12}CO and ^{13}CO available to the RLT should reveal more cool gas for which the THz CO transitions can tightly constrain the conditions.

This map demonstrates that it is possible to make reliable observations from the ground in a region of the electromagnetic spectrum normally considered to be inaccessible. In the near future we hope to begin observations at higher frequencies to make use of the other atmospheric windows available from our site.

We would like to thank Leonardo Bronfman and Jorge May of the Universidad de Chile for invaluable support and assistance with this project. We also thank Joseph Salah and Mike Poirier of the MIT Haystack Observatory for support during the assembly and testing of the RLT at the Westford Radio Telescope. We are grateful for the continuous support we have received from the Director of SAO, Irwin Shapiro. K. N. Allers, A. L. Betz, and T. W. Wilson have been kind enough to provide us with access to their data. We would like to thank the anonymous referee for many improvements to the paper. D. P. M. acknowledges support from an NSF Graduate Research Fellowship.

REFERENCES

- Becklin, E. E. & Neugebauer, G. 1967, *ApJ*, 147, 799
 Betz, A. L. & Boreiko, R. T. 1993, in *ASP Conf. Ser.* 41, *Astronomical Infrared Spectroscopy: Future Observational Directions*, ed. S. Kwok (San Francisco: ASP), 349
 Blake, G. A., Masson, C. R., Phillips, T. G., & Sutton, E. C. 1986, *ApJS*, 60, 357
 Blundell, R., et al. 2002, in *13th International Symposium on Space Terahertz Technology*, ed. C. E. Tong & R. Blundell, 159–166
 Castets, A., Duvert, G., Dutrey, A., Bally, J., Langer, W. D., & Wilson, R. W. 1990, *A&A*, 234, 469
 Dougados, C., Lena, P., Ridgway, S. T., Christou, J. C., & Probst, R. G. 1993, *ApJ*, 406, 112
 Downes, D., Genzel, R., Becklin, E. E., & Wynn-Williams, C. G. 1981, *ApJ*, 244, 869
 Flower, D. R. & Launay, J. M. 1985, *MNRAS*, 214, 271
 Gezari, D. Y., Backman, D. E., & Werner, M. W. 1998, *ApJ*, 509, 283
 Goldsmith, P. F., Bergin, E. A., & Lis, D. C. 1997, *ApJ*, 491, 615
 Greenhill, L. J., Gwinn, C. R., Schwartz, C., Moran, J. M., & Diamond, P. J. 1998, *Nature*, 396, 650
 Herrmann, F., Madden, S. C., Nikola, T., Poglitsch, A., Timmermann, R., Geis, N., Townes, C. H., & Stacey, G. J. 1997, *ApJ*, 481, 343
 Howe, J. E., Jaffe, D. T., Grossman, E. N., Wall, W. F., Mangum, J. G., & Stacey, G. J. 1993, *ApJ*, 410, 179
 Ikeda, M., Oka, T., Tatematsu, K., Sekimoto, Y., & Yamamoto, S. 2002, *ApJS*, 139, 467
 Kawamura, J., et al. 2002, *A&A*, 394, 271
 Kleinmann, D. E. & Low, F. J. 1967, *ApJ*, 149, L1
 Langer, W. D. & Penzias, A. A. 1990, *ApJ*, 357, 477
 Marrone, D. P., Blundell, R., Gibson, H., Paine, S., Papa, D. C., & Tong, C.-Y. E. 2004, in *15th Int. Symp. on Space Terahertz Technology*, ed. G. Narayanan (Amherst, MA: Univ. Mass. Press), in press, preprint (astro-ph/0406290)
 Matsushita, S., Matsuo, H., Pardo, J. R., & Radford, S. J. E. 1999, *PASJ*, 51, 603
 Meledin, D. et al. 2004, *IEEE Transactions on Microwave Theory and Techniques*, in press
 Menten, K. M. & Reid, M. J. 1995, *ApJ*, 445, L157
 Paine, S., Blundell, R., Papa, D. C., Barrett, J. W., & Radford, S. J. E. 2000, *PASP*, 112, 108
 Plambeck, R. L., Wright, M. C. H., Mundy, L. G., & Looney, L. W. 1995, *ApJ*, 455, L189
 Plume, R., et al. 2000, *ApJ*, 539, L133
 Rodríguez-Franco, A., Wilson, T. L., Martín-Pintado, J., & Fuente, A. 2001, *ApJ*, 559, 985
 Röser, H. 1991, *Infrared Physics*, 32, 385
 Schilke, P., Benford, D. J., Hunter, T. R., Lis, D. C., & Phillips, T. G. 2001, *ApJS*, 132, 281
 Schulz, A., et al. 1995, *A&A*, 295, 183
 Scoville, N. Z. & Solomon, P. M. 1974, *ApJ*, 187, L67
 Sempere, M. J., Cernicharo, J., Lefloch, B., González-Alfonso, E., & Leeks, S. 2000, *ApJ*, 530, L123
 Stacey, G. J., Jaffe, D. T., Geis, N., Genzel, R., Harris, A. I., Poglitsch, A., Stutzki, J., & Townes, C. H. 1993, *ApJ*, 404, 219
 Stutzki, J. & Winnewisser, G. 1985, *A&A*, 144, 13
 Sutton, E. C., Blake, G. A., Masson, C. R., & Phillips, T. G. 1985, *ApJS*, 58, 341
 Tan, J. C. 2004, *ApJ*, 607, L47
 Tauber, J. A., Tielens, A. G. G. M., Meixner, M., & Foldsmith, P. F. 1994, *ApJ*, 422, 136
 Tigges, A. 1993, PhD thesis, Universität zu Köln
 Ulich, B. L. & Haas, R. W. 1976, *ApJS*, 30, 247
 van der Werf, P. P., Stutzki, J., Sternberg, A., & Krabbe, A. 1996, *A&A*, 313, 633
 Walmsley, C. M., Natta, A., Oliva, E., & Testi, L. 2000, *A&A*, 364, 301
 Wilson, T. L., Muders, D., Kramer, C., & Henkel, C. 2001, *ApJ*, 557, 240 (WMKH01)
 Wright, M. C. H., Plambeck, R. L., Vogel, S. N., Ho, P. T. P., & Welch, W. J. 1983, *ApJ*, 267, L41

TABLE 1
LINE PEAK TEMPERATURES USED IN LVG MODEL FITTING

Position ^a	T _{9→8} ^{12 b}	T _{7→6} ^{12 c}	T _{6→5} ^{12 d}	T _{4→3} ^{12 c}	T _{3→2} ^{12 e}	T _{3→2} ^{13 e}	T _{1→0} ^{13 f}
1	85±21	137±34	83±21	102±26	93±23	24±6	11±3
2	80±20	120±30	...	102±26	86±22	24±6	11±3
3	36±9	...	46±12	...	71±18	12±3	7.0±1.8
4	27±7	...	56±14	...	74±19	30±7	13±3

NOTE. — Line peak temperatures labeled as T_Y^X, where X is the carbon isotope and Y is the rotational transition. All values are in Kelvins.

^aSee labeled positions in Figure 1.

^bData from this work.

^cData from WMKH01.

^dData from K. N. Allers 2005, in preparation.

^eData from Tigges (1993).

^fData from Plume et al. (2000).

TABLE 2
GAS PARAMETERS DERIVED FROM LVG MODEL

Position	T _{kin} (K)	log n (cm ⁻³)	log(dN/dv) (cm ⁻² s km ⁻¹)	χ _{r,min} ²
1	120±20	3.5 – 4.6 ^a	18.0 ± 0.2	0.83
2	120±20	3.5 – 4.3 ^a	18.0 ± 0.2	0.81
3	70±10	4.1 ± 0.3	17.7 ± 0.2	1.46
4	70±10	3.8 ± 0.3	18.1 ± 0.2	1.16

^aPoorly constrained upper limit. See text for details.